Enhancing the mechanical and hydraulic properties of coarse quartz sand using a water-soluble hydrogel based on bacterial alginate for novel application in agricultural contexts

Authors: Cesar Barrientos-Sanhueza[1], Pedro Mondaca[1], Miguel Tamayo[1], Juan E. Álvaro[1], Alvaro Díaz-Barrera[2], Italo F. Cuneo[1]*

[1]Facultad de Ciencias Agronómicas y de los Alimentos, Pontificia Universidad Católica de Valparaíso, Valparaíso 2340025, Chile.
[2]Escuela de Ingeniería Bioquímica, Pontificia Universidad Católica de Valparaíso, Valparaíso, Valparaíso 2340025, Chile.

***Corresponding author:**
Italo F. Cuneo
Phone: 56 32 2372913; Email: italo.cuneo@pucv.cl

ABSTRACT

Climate change is generating severe changes in the physical behavior of soils (i.e. soil structure, mechanical resistance, and water conductivity), causing negative impacts on different agricultural systems and, therefore, threatening food security. To cope with this situation, hydrogels based on biopolymers have been proposed to modify the mechanical and hydraulic behavior of complex porous materials such as soils, yet most of them are non-soluble making their application at field level laborious. In here, we investigated the effect of a water-soluble hydrogel based on bacterial alginate on the mechanical and hydraulic behavior of coarse quartz sand. The results from unconfined uniaxial compression test (UCCT) showed that the strength of the sand treated with hydrogel increased by 94.5%, while the hydraulic conductivity decreased 33%. Interestingly, we observed that bacterial alginate and hydrogel shifted the mechanics of the fluid phase towards a Darcy regime. The aggregate stability tests showed that coarse quartz sand treated with hydrogel display larger mean weight diameter (MWD) reaching 1.5 mm compared to 0.12 mm of the control (i.e. coarse quartz sand). Finally, transmission light microscopy

This article has been accepted for publication and undergone full peer review but has not been through the copyediting, typesetting, pagination and proofreading process, which may lead to differences between this version and the Version of Record. Please cite this article as doi: 10.1002/saj2.20315.

imaging of the hydrogel treatment revealed a new 3-D matrix between the quartz sand particles, changing the micro and macro aggregates and providing a modified structure of the sand material. Our findings suggest that the use of the water-soluble hydrogel improve the mechanical and hydraulic behavior of coarse quartz sand, allowing better soil conservation against climate change related phenomena, but also potentially applicable in agricultural systems facing water scarcity.

HIGHLIGHTS

- Coarse sand strength increased using alginate hydrogel.
- Hydraulic behavior is modified by bacterial alginate and hydrogel.
- Aggregate stability is significantly improved by hydrogel application.
- A new 3-D matrix (hydrogel-sand) was revealed.

Key words: Soil mechanical and hydraulic behavior; bacterial alginate; hydrogel; aggregate stability of soils.

1. INTRODUCTION

Soil erosion and water scarcity are serious threats facing world food production (Lal, 2001; Pimentel and Burgess, 2013; Borrelli et al., 2017), and climate change trends indicate that this problem will worsen in several agricultural regions worldwide (Vicuña et al., 2012; Borrelli et al., 2017; Garreaud et al., 2017). The magnitude of these threats is related to soil physical properties, such as soil structure, mechanical resistance, and water conductivity (Bronick, 2005; Carminati et al., 2009; Rabot, 2018). Thus, the improvement of soil physical properties is crucial in agricultural systems facing climate change; increasing the overall resilience of the food production sector (e.g. Barzegar, 2003; Singh, 2018).

Soil functionality is, to a large degree, governed by soil structure (Lal, 2001; Schlüter, 2020), which is understood as the arrangement of soil particles forming a complex porous material composed of soil aggregates (Hillel, 2003; Aleklett et al., 2018). Aggregates are the structural unit of soils and their stability constitute a cornerstone parameter of soil quality (Menon, 2020). In agricultural systems, the process of soil aggregation is crucial since: 1) facilitate the movement of water, gas

and solutes in the soil profile; 2) enhance soil aeration; 3) enhance soil infiltration and water storage; and 4) reduce evaporation, run-off, and erosion; providing optimal conditions for plant growth (Carminati et al., 2009). Mechanical behavior of soils are scarcely considered in agricultural research, yet they are important properties in agricultural systems since they have an influence on soil compaction and tillage (Verruijt, 2018; Ghezzehei, 2012) and they are related to erodibility (i.e. soil resistance to erosion; Keersebilck, 1990; Ghezzehei, 2012). Soil compaction as well as soil erosion by wind and water are classified as the most harmful processes in agricultural systems (Horn and Peth, 2012). Soil deformation as the sum of soil compaction and shear processes leads to numerous environmental changes affecting soil functions such as: 1) soil infiltration and water storage, 2) trace gas emissions, and 3) soil erosion and nutrient loss (Taylor and Ratliff, 1969; Horn and Peth, 2012; Alameda et al., 2012).

The effects of the mechanical stresses over the soil strongly depends on the configuration and composition of soil particles and, especially, soil aggregates (Taylor and Ratliff, 1969; Hillel, 2003; Alameda et al., 2012). For example, sandy soils that have a single grain structure and are very important in many agricultural regions of the world, can be affected by wind erosion generating *in situ* soil losses (Lyles, 1977; Tatarko, 2001). Besides, soils can be deformed when are subjected to compression and tension forces in tillage processes (i.e. contact forces that are transmitted among soil particles; Verruijt, 2018). Similar deformation happens in clay soils during drying periods when individual clay particles release water in layers, generating compression through compaction of the soil aggregates (Stewart et al., 2016). Therefore, taking care of the configuration and composition of the soil aggregates is a key factor to minimize the impacts of mechanical stresses and water scarcity, increasing the resilience of agricultural systems. Also, the configuration of aggregates (i.e. macro and micropores rates) influence water flow through the soil (Radcliffe and Šimunek, 2012). One part of the water that infiltrates in the soil returns to the atmosphere trough evaporation, and the other part may be taken by plant roots and eventually returned to the atmosphere via plant transpiration (Philip, 1966; Radcliffe and Šimunek, 2012; Carminati et al., 2012). However, soil erosion caused by the absence of soil aggregates often lead to poor hydraulic conductivity (Tatarko,

2001; Hillel, 2003; Radcliffe and Šimunek, 2012), limiting water availability for plants (Hillel, 2003; Carminati et al., 2012; Radcliffe and Šimunek, 2012).

To control and improve the mechanical behavior of soils under different environmental stresses, several porous materials (i.e. soil amendments) based on hydrogels have been developed to mimic some of the physical effect of natural polymers (i.e. root mucilage exhibiting glue-like behavior) to bind sand, silt, and clay particles together (Hillel, 2003). Some of these hydrogels are based on chitosan (Hataf et al., 2018), brown seaweed alginate (Wen et al., 2019), polyacrylamide (Kumar and Saha, 2011; Lentz, 2015), and anionic xanthan gum (Chang et al., 2015). Hydrogels are notable as they have been reported to be capable of modifying the mechanical behavior of soils by increasing the water holding capacity by altering the mechanics of the fluid phase (Chang et al., 2015; Hataf et el., 2018; Wen et al., 2019; Benard et al., 2019). In this regard, the remanent stiff filaments of hydrogel-sand composite materials of drying soils are one of the most important alteration of the mechanics in the fluid phase, and the Ohnesorge number elegantly describes the phenomenon (Benard et al., 2018). The Ohnesorge number (Oh) describes how the viscosity acts like a buffer on the motion caused by surface tension (Benard et al., 2018). The lower the Oh number (i.e. $Oh << 1$) the weaker are the friction losses due to viscous forces, which means that surface tension is the dominating force. The higher the Oh number (i.e. $Oh >> 1$) the more dominant is the internal viscous dissipation, indicating the great importance of viscous forces (Benard et al., 2018). In the present work the Oh number helps to understand the persistence of the liquid bridges between the alginate and hydrogel treatments and the coarse quartz sand particle surfaces (Benard et al. 2018; Benard et al., 2019; Krainer et al., 2019).

Up to date, the most used hydrogels are composed of synthetic polymers and copolymers, such as polyacrylamide (Xu et al., 2015; Cao et al., 2017) and polyacrylates (Narjary et al., 2012; Xu et al., 2015; Liu and Chan, 2015). However, it has been suggested that the chemical base of these hydrogels (i.e. acrylamide) is potentially harmful to the environment and humans due to the accumulation of these chemical compounds in subterranean water bodies or in the surface layers of the soil (Konings, 2003; FAO, 2003; Weston et al., 2009; Lai et al., 2017; Lu et al., 2018;

Dasari et al., 2018). As an alternative, one strategy is the implementation of polymers obtained from plants or microorganisms to create a new type of hydrogels with low environmental-health impacts (Guilherme et al., 2015). One of these natural polymers is the bacterial alginate that can be produced and obtained through the cultivation and bioprocessing of the bacterium *Azotobacter vinelandii*, (Díaz-Barrera and Soto, 2010; Urtuvia et al., 2017). Bacterial alginate is a polysaccharide with a linear chain consisting of 1→ 4 linked β-$_D$-mannuronic acid (M) and its C-5 epimer α-$_L$-guluronic acid (G) (Pawar and Edgar, 2012). Improvement of the ionic gel strength can be produced by the addition of covalent crosslinking (Pawar and Edgar, 2012) using divalent cations reactions with the bacterial alginate in form of chelates, generating new junctions` points (Sikorski et al., 2007). Ca^{+2} is the most commonly used cation to create the Ca-alginate hydrogel (Pawar and Edgar, 2012). This mix has been used in construction, biomedical engineering, and food areas (Draget et al., 2005; Díaz-Barrera and Soto, 2010; Guilherme et al., 2015; Urtuvia et al., 2017). Yet, the effect of this new bacterial alginate-based hydrogel over the mechanical and hydraulic behavior of complex porous materials such as coarse quartz sand has not been explored in the past.

In this study, we hypothesized that the addition of a new hydrogel based on bacterial alginate to coarse quartz sand has positive effects on mechanical (i.e. soil strength, aggregate stability) and hydraulic properties (hydraulic conductivity). We used coarse quartz sand (i.e. grain diameter between 0.063 – 2 mm) because of three main reasons: 1) it is highly susceptible to mechanical compressive stresses; 2) it is highly porous (i.e. permeable to water), then it has a low water holding capacity; and 3) it has no stability of aggregates (i.e. single grain structure)(Hillel, 2003; Ghezzehei, 2012; Verruijt, 2018). To test our hypothesis, we used unconfined uniaxial compression tests, falling head permeability tests, aggregate stability tests, and transmission light microscopy.

2. MATERIAL AND METHODS

2.1 Porous media particle size distribution

Quartz sand (MIGRIN S.A. non-metallic mining) was used in this study for its physical properties (i.e. highly susceptible to mechanical compressive stresses;

highly permeable to water; and lack of stability of aggregates; Hillel, 2003; Verruijt, 2018; Ghezzehei, 2012). The sieve analysis method was used to determine particle size distributions following the ASTM C136 (ASTM, 2013; Wen et al., 2019) and using a standard U.S. sieve (C-tech Instruments, India). The sand particle distribution curve showed that the sand used in this study is mainly made up of 55.46% of particles with a particle size of 0.5 mm, 37.95% of 0.25 mm, 5.5% of 0.15 mm, and 1.09% of 0.053 mm (Fig. 1). The coefficient of uniformity (C_u) was 2.36 and the coefficient of gradation (C_c) 0.88. The sand was classified as coarse grained and poorly graded (SP) according to Unified Soil Classification System (USCS, 1986).

2.2 Bacterial alginate production from *Azotobacter vinelandii*

Bacterial alginate was fermented and recovered in several steps. The fermentation stage consisted in the cultivation of the bacteria *Azotobacter vinelandii* ATCC 9046 in a culture medium composed of sucrose as carbon source and under atmospheric nitrogen fixation. The bacterial alginate production was carried out in a 30 L bioreactor (Infors HT, Techfors, Switzerland). The 30 L bioreactor operated at 300 rpm, 1 vvm, 30ºC and pH 7.0 controlled with NaOH (2N) (Padilla-Córdova et al., 2020). Samples of culture broth (30 mL) were mixed with 6 mL of Na_4EDTA (0.1 M) and NaCl (1.0 M) and then centrifuged at 7650 × g over 10 min. The obtained pellet was separated, and the supernatant was used to recuperate the alginate. A 3:1 volume of cold propan-2-ol was added to the supernatant, and the resultant precipitate was filtered through 0.45-µm Millipore filter paper, dried at 60°C to a constant weight, and then ground and weighed. The final product resulted in a solid stable product with a molecular weight of 453 ± 42 kDa. (Díaz-Barrera et al., 2017). Finally, the bacterial alginate was recovered and allowed to dry in an oven at 60°C for 24 hours resulting in a chemically stable product (i.e. lack of chemical reactions such as oxidation, polymerization, and hydrolysis) until rehydration.

2.3 Quantification of the contents of mannuronic and guluronic acid in alginate by Fourier transform infrared (FTIR) spectroscopy

The quantification of the content of mannuronic and guluronic acid in alginate was carried out using a FTIR with the technique of total attenuated reflectance (ATR). Alginate sample was freeze-dried prior to FTIR measurements. FTIR

analyses were recorded from 500-4000 cm^{-1} using a Jasco FT/IR-4600 spectrometer. 64 scans were collected with a resolution of 4 cm^{-1} (Leal et al., 2008). Supplementary figure 1 shows the obtained IR spectra of bacterial alginate. It was possible to identify at 1612 cm-1 and 1392 cm-1 the stretching vibrations of the COO- group characteristic of alginate structure. Moreover, the stretching vibrations of the CO group than correspond to bond of guluronic (G) and mannuronic (M) acids were identified to 1314 cm-1 and 1290 cm-1, respectively (Sartori et al., 1997). Finally, the IR data was used to calculate G/M ratio. G/M ratio was calculated by dividing the transmittance obtained of the absorption bands in 1320 cm-1 and 1290 cm-1 (Sartori et al., 1997). The IR data were analyzed using Bio-Rad software (version 18.3.1).

2.4 Preparation of Ca-alginate hydrogel

In this study, we used $Ca(OH)_2$ for its higher solubility (Stephen and Stephen, 1962). When $Ca(OH)_2$ is mixed with water, the covalent ions of Ca^{+2} are released to the medium, leaving them available to create the Ca-alginate porous complex (i.e. hydrogel). The bacterial alginate was solubilized in distillated (DI) water using a magnetic stirrer (AccuPlate™ Hotplate Stirrer, Labnet, USA) creating a water-soluble solution. Then a solution of $Ca(OH)_2$ at 0.5 M (i.e. 37.04 g/L) were solubilized in DI water using a magnetic stirrer (AccuPlate™ Hotplate Stirrer, Labnet, USA) (Wen et al., 2019). Finally, the bacterial alginate and $Ca(OH)_2$ solution were added to the quartz sand and mixed by hand to accomplish the homogeneity of the Ca-alginate hydrogel.

2.5 Sample preparation

All the experiments were carried out at the Soft Matter Biophysics lab in the School of Agronomy PUCV, Chile. Four treatments were performed to test the individual effects of the components that conformed the hydrogel. The treatments were: (I) control consisting on DI water, (II) calcium hydroxide ($Ca(OH)_2$), (III) bacterial alginate, and (IV) the mix of calcium with the bacterial alginate (i.e. Ca-alginate hydrogel). The same treatments were used in every experiment performed in this study. The bacterial alginate, the calcium hydroxide, and the mix of them (i.e. Ca-alginate hydrogel) treatments were applied independently. The Ca-alginate

hydrogel was applied and mixed with the samples to create an *in situ* effect on the coarse quartz sand.

For the unconfined uniaxial compression and falling head permeability tests, the samples were prepared using an adaptation of the following sample preparation methodology (Wen et al., 2019): 1) 800 g of coarse quartz sand were weighed on plastic pots; 2) the treatments previously prepared were applied in liquid form (i.e. water-soluble solutions) over the weighted sand and then mixed by hand for 1 min to homogenize the samples (Supporting information Fig. S2). For practical purposes bacterial alginate concentration was estimated according to the weight/weight (w/w) ratio of the coarse quartz sand. At 800 g of sand, 0.8 g of bacterial alginate was applied in a water-soluble solution that equals to 0.1% (w/w). The volume of water applied was determined according to the saturation point of the sand (i.e. field capacity) which was 150 ml of water. Finally, the curing time was 3 days to ensure that the treatments had the same reaction times with the coarse quartz sand (Hataf *et al*., 2018; Wen *et al*., 2019).

2.6 Unconfined uniaxial compressive testing

A texture analyzer (Model Ta.XT *plusC*, Stable Micro Systems Ltd, England) equipped with a compression plate of 100 mm of diameter (TMS 100 mm diameter, p/100) was used over cylindrical specimens of 70 mm in diameter × 160 mm height. Before the compression test, the treatments were compacted in a custom-made mold of polyvinyl chloride (PVC)(see supporting information Fig. S3). The texture analyzer parameters were set as follows: 1) the trigger threshold (i.e. force) was set at 0.05 N, 2) pre-test = 1 mm s^{-1}, 3) speed test = 1 mm s^{-1}, 4) post-test = 10 mm s^{-1}, and 5) the compression force was recorded in Newton (N) at 20 mm deformation. Then, the data were transformed into Mega Pascals (MPa) and percentage of axial strain (%). The elastic behavior, the deformation at break, and the maximum strength of treated coarse quartz sand (i.e. maximum resistance until the soil breaks) were obtained to measure the stress-strain relationship. The Young´s modulus (i.e. module that indicates how elastic it is a body) was calculated using the slope of the elastic zone of the stress-strain curves (n = 6). Finally, fracture point (i.e. point at which the soil breaks) was calculated using the slope angle (θ) of the elastic zone at

the point of fracture after the maximum resistance of the samples (Supporting information Fig. S4).

2.7 Aggregate stability measurement

Aggregate stability measurements were based on the work proposed by Narjary and Aggarwal (2014), and Le Bissonnais (2016). The mechanical breakdown by shaking after pre-wetting method was used for this test. The objective of pre-wetting is to test the wet mechanical cohesion of aggregates independently of slaking (Le Bissonnais, 2016). The experimental unit consisted of plastic pots of 250 g of coarse quartz sand. In addition, the bacterial alginate and Ca-alginate hydrogel treatments were applied at a concentration of 0.1% (w/w) ratio of coarse quartz sand. Each treatment was performed with six replications. Each experimental unit were exposed to 20 cycles of wetting (field capacity) and drying (permanent wilting point) for three weeks. Mechanical breakdown by shaking after pre-wetting method were applied for each experimental unit. The samples were oven dried (BOV-C30T, BioBase Biodustry, Jinan, China) at 60ºC for 24 h and then screened using seven sieves (2000 µm, 1000 µm, 500 µm, 250 µm, 125 µm and 53 µm, respectively). Mass was recorded after drying. Finally, the mean weight diameter (MWD) was calculated as an index of aggregation using the next formula (Le Bissonais, 2016):

$$MWD = \sum_{i=1}^{n} XiWi \quad (1)$$

where MWD is (g/mm), X_i is the weight of dry coarse quartz sand in the sieve *i* (g), and W_i is the average diameter of the pores of the adjacent sieve meshes (mm).

2.8 Hydraulic conductivity test

The falling head permeability method was implemented following the ASTM D5084-16a protocol (ASTM-D5084-16a, 2016). After sample preparation, three consecutive falling head experiments (i.e. flushing events) were conducted on saturated samples in the head permeability test set (HM-891, Gilson Company INC., Ohio, USA). The average of the three flushing events was used to compute saturated hydraulic conductivity (*K*) from falling head by using the Darcy´s law equation (Barnes et al., 2014):

$$K = \frac{aL}{A(\Delta t)} * Ln\left(\frac{h_0}{h_1}\right) \quad (2)$$

Where, a is the cross-sectional area of standpipe (m), L is the length of specimen (m), A is the cross-sectional area of specimen (m), Δt is time elapsed (s), h_0 and h_1 are the initial and final water meniscus heights of the water column (m). To verify the flow regime, we estimated the Reynolds number for each treatment as:

$$Re = \frac{\rho v D_p}{\mu} \quad (3)$$

where ρ is the density of the fluid (kg m^{-3}), v is the flow speed (m s^{-1}), D_p is the diameter of particles of the coarse quartz sand (mm) and μ is the dynamic viscosity of the fluid (Pa·s). When non-Darcy flow was found, we approximated the Forchheimer's equation:

$$-\frac{\Delta P}{L} = \frac{\mu}{k} v + \rho \beta v^2 \quad (4)$$

where k is the Forchheimer permeability (m^2), β correspond to the Forchheimer coefficient or non-Darcy flow coefficient (m^{-1}). Then, rearranging the equation (4) as:

$$\frac{\Delta P}{L v \mu} = \frac{1}{k} + \beta \left(\frac{\rho v}{\mu}\right) \quad (5)$$

we created a Forchheimer plot relating $\frac{\Delta P}{L v \mu}$ vs $\frac{\rho v}{\mu}$, obtaining a straight line with slope β and $\frac{1}{k}$ as intercept. We then estimated the Forchheimer number (F_0) as $F_0 = \frac{k \beta \rho v}{\mu}$ and the non-Darcy effect E as $E = \frac{F_0}{1+F_0}$ (Bear, 1972; Comiti et al., 2000; Zeng and Grigg, 2006; Huang and Ayoub, 2008). In the present work, the Ohnesorge number (Oh) helps to understand the persistence of the liquid bridges between the alginate and hydrogel treatments and the coarse quartz sand particle surfaces, and was estimated according to equation (6):

$$Oh = \frac{\mu}{\sqrt{\rho \sigma L}} \quad (6)$$

where μ dynamic viscosity of the fluid (Pa·s), ρ is the density of the fluid (kg m^{-3}), σ is the surface tension (N m^{-1}) and L is the characteristic length scale of the filaments of hydrogel between soil particle surfaces (m) (Benard et al., 2019).

2.9 Transmission light microscopy imaging

Transmission light microscopy imaging was used to observe in detail the structure formed in the porous matrix by the interaction of the different treatments with the coarse quartz sand. The ability of the Ca-alginate hydrogel to swell and absorb water allow us to use a blue ink-water solution (e.g. pen ink) to identify the structure of the new matrix (Benard et al., 2017). To visualize the treatments under the microscope, glass slides were used to hold the samples of the treated coarse quartz sand. The blue ink-water solution is absorbed by the Ca-alginate hydrogel, adhering to the physical bond of the hydrogel and allowing its visualization under transmission light microscopy. The mix of the different treatments with the ink-water solution had a gravimetric ratio of 1:2 and was done at free hand (not submerged) with a micropipette of 200 µm (Benard et al., 2017). Samples were observed using Leica DMIL LED inverted microscope (Leica Microsystems, Wetzlar, Germany). Images were acquired with a Leica MC170HD digital camera.

3. Statistical analysis

Analysis of variance (ANOVA) was performed using R version 4.0.0 statistical computing environment (R Core Team, 2020) with the aid of the CAR software package (Fox & Weisberg, 2011). The Shapiro–Wilk and Levene tests were used to check for normality and homogeneity of variance, respectively. Tukey' honest significant difference test was used to determine significant differences among treatments.

4. RESULTS

4.1 Unconfined uniaxial compressive testing (UUCT)

We used unconfined uniaxial compressive testing to quantify the effects of the different treatments (i.e. (I) control, (II) calcium hydroxide ($Ca(OH)_2$), (III) bacterial alginate, (IV) Ca-alginate hydrogel) on the stress-strain relationship, the elastic behavior, and the deformation at break of treated coarse quartz sand (Fig. 2A, B, C) (Leite and Ferland, 2001). Coarse quartz sand under control treatment displayed stress-strain curves with higher Young´s modulus (173 ± 46.2 MPa SE) reaching almost 2-fold compared with Ca-alginate hydrogel treatment (73.7 ± 5.3 MPa SE) and bacterial alginate (64.2 ± 7.2 MPa SE) (Fig. 2A, B). The Young´s modulus of the

coarse quartz sand treated with calcium hydroxide (156.9 ± 14.5 MPa SE) was similar to the one observed in the control. During data collection, axial deformation progressively increased until reaching the point of deformation at fracture (see Fig. 2C). The mean axial deformation (%) was 1.9, 3.8, 4.1, and 5, respectively for treatments control, calcium hydroxide ($Ca(OH)_2$), bacterial alginate, and Ca-alginate hydrogel. In the present study, the maximum compressive stress reached more than 3.0 MPa, exceeding 5% of axial deformation. Significant differences were found among treatments in percentage of axial deformation at fracture (%; p = 0.0019) where the Ca-alginate hydrogel treatment showed fracture at 6.4% axial deformation while control and calcium hydroxide treatments displayed fracture at 3.7% and 3.5% axial deformation respectively (Fig. 2C). The bacterial alginate treatment showed fracture at 4.2% axial deformation, having an intermediate effect between the Ca-alginate and control - calcium hydroxide treatments (Fig. 2C). Overall, the resistance to fracture of the coarse quartz sand cylinders increased by 74% in Ca-alginate treatment compared to control treatment.

4.2 Aggregate stability test

We used the aggregate stability test to quantify the mechanical disruption of coarse quartz sand treated with the different Ca-alginate hydrogel compounds. The analysis was done accordingly to the classes of stability proposed by Le Bissonais (2016). In this study, to control confounding factors, only the first three meshes were used (i.e. 2000 µm, 1000 µm, and 500 µm) to perform the aggregate stability test since most of the particles diameters were located in the 500 µm and 125 µm sieves. In this way, we recorded the generation of macroaggregates, avoiding the particles size fraction (i.e. 500 µm, 250 µm, 125 µm, and 53 µm) that the coarse quartz sand already has. Coarse quartz sand under Ca-alginate hydrogel treatment shows a prominent aggregate stability (1.5 ± 0.4 mm/g SE) compared to the control treatment (0.1 ± 7.0 e^{-3} mm/g SE), calcium hydroxide treatment (0.1 ± 4.0 e^{-3} mm/g SE), and bacterial alginate treatment (0.2 ± 6.0 e^{-2} mm/g SE). Significant differences of aggregate stability were found among treatments (p = 0.0003179) (Fig. 3).

4.3 Hydraulic conductivity test

We used the falling head permeability test to quantify the effects of the different Ca-alginate hydrogel compounds over the coarse quartz sand saturated hydraulic conductivity (*K*). As shown in Fig. 4A, bacterial alginate and Ca-alginate hydrogel treatments lay into the Darcy's model's regime of the flux density-hydraulic gradient relation displaying relatively low Reynolds numbers (Re ≈ 0.02) while the control and calcium treatments showed a non-Darcy flow regime with Re ≈12.0, F_0 ≈ 2.46 and E ≈ 0.7. Saturated hydraulic conductivity was significantly reduced in the Ca-alginate hydrogel and bacterial alginate treatments compared with the control and calcium treatments (p = 0.0001482; Fig. 4B). The Ca-alginate hydrogel treatment achieved to reduce the saturated hydraulic conductivity by 32% compared to the control treatment. Coarse quartz sand mean K values were separated in two groups, (1) control and calcium hydroxide treatments showed higher values (2.7 ± 1.7 e^{-3} SE m s^{-1} and 2.4 ± 1.6 e^{-3} SE m s^{-1}), and (2) bacterial alginate and Ca-alginate hydrogel treatments showed lower values (1.5 ± 1.0 e^{-3} SE m s^{-1} and 1.8 ± 1.8 e^{-3} SE m s^{-1}). Finally, the Oh numbers estimated for control and calcium treatments were ≈ 0.2, and for the bacterial alginate and Ca-alginate hydrogel treatments ≈ 83.1 – 83.3 respectively.

4.4 Transmission light microscopy imaging

We obtained 90 transmission light microscopy images to observe in detail the effects of the different treatments over the structure and particle configuration of treated coarse quartz sand. A representative image was selected for every treatment. The control and calcium treatments showed direct contact between the quartz sand particles, but without external connections of any kind (Fig. 5A, B). On the other hand, the bacterial alginate treatment displayed new links (i.e. hollow cylinders) at interparticle level in the coarse quartz sand (Fig. 5C). Finally, our images revealed that the structures of Ca-alginate hydrogel treatment were larger, because instead of filaments (i.e. hollow cylinders), a three-dimensional network was created, generating a new matrix of Ca-alginate hydrogel-coarse sand particles (Fig. 5D).

5. DISCUSSION

In this study, mechanical and hydraulic behavior of coarse quartz sand treated with bacterial alginate-based hydrogel were evaluated for potential application in agricultural systems facing climate change related phenomena such as wind erosion, heavy rainfall, flooding, and drought. The results from unconfined uniaxial compression test (UCS) showed that the strength of the sand treated with the Ca-alginate hydrogel increased by 94.5%, while the hydraulic conductivity decreased by 33%. The Ca-alginate hydrogel and bacterial alginate treatments displayed a Darcy flow regime while control and calcium lay on the non-linear part of the flux density-hydraulic gradient relation displaying a Forchheimer flow regime (i.e. water flow more easily in the macropores inside the coarse quartz sand particles). Also, Oh number of the Ca-alginate hydrogel and bacterial alginate treatments (Oh>>1) indicates that viscous forces dominates over inertia and surface tension forces, helping to maintain the hydraulic connection through the filamentous network created by the alginate and Ca-alginate hydrogel treatments in the coarse quartz sand. The aggregate stability tests showed that sand aggregates were greatly improved with the Ca-alginate hydrogel displaying larger mean weight diameter (MWD) of 1.5 mm/g. Such improvement on the stability of soil aggregates could play a key role in agricultural systems facing the effects of climate change (e.g. soil erosion and low water availability). Finally, transmission light microscopy imaging of the Ca-alginate hydrogel treatment revealed a new 3-D matrix between the polymer chains of the bacterial alginate hydrogel and the quartz sand particles surfaces, changing the micro and macro aggregates and providing an improved structure of the coarse quartz sand. The results presented here provide evidence that use of this new Ca-alginate hydrogel based on bacterial alginate improve the mechanical and hydraulic behavior of coarse quartz sand, a poor-quality coarse quartz sand in term of structure and hydraulic behavior; highlighting that this amendment may be particularly beneficial in agricultural systems facing climate change and their related phenomena (i.e. soil erosion and low water availability).

The stress-strain relationship defines the coarse quartz sand strength (i.e. maximum amount of stress a solid can withstand before it fails) and elasticity

behavior. These two variables are key mechanical determinants of whole coarse quartz sand functionality and quality in agricultural contexts (Hillel, 2003; Horn and Peth, 2012). Changes in mechanical behavior of sandy soils mixed with different hydrogel types have been studied in the past (Chang and Cho, 2012; Chang et al., 2015; Chang et al., 2016; Hataf et al., 2018; Wen et al., 2019). In those previous studies, the percentage of axial strain and the maximum compressive stress did not exceed 5% and 2.5 MPa, respectively (Chang et al., 2015; Hataf et al., 2018; Wen et al., 2019). Our data, however, showed that the maximum compressive stress achieved more than 3.0 MPa exceeding 5% of axial strain (Fig. 2a). Also, the mechanical behavior of the coarse sand treated with Ca-alginate hydrogel revealed a change in the elastic modulus compared to the control (See. Fig. 2A, B). The Young's modulus in our control treatment was consistent with previous reported data for granular material such as coarse sand (Obrzud and Truty, 2012). In here, the application of bacterial alginate and Ca-alginate hydrogel treatment reduced the Young's modulus in almost 2-fold compared to the control treatment; meaning that the treated sand became more flexible, changing its shape considerably compared to the control when applying the same stress load.

When a mechanical stress is applied, soil deformation occurs first at the weakest point in the soil matrix. Then, further increases in stress result in the formation of failure zones (Horn and Peth, 2012; see supporting information Fig. S4). In here, axial strain at fracture (%) of the Ca-alginate hydrogel treatment doubled the strain fracture resistance of quartz sand compared with the other treatments, suggesting an improvement in the soil strength. This could be explained by the effective cohesion/adhesion effect of the Ca-alginate hydrogel with the sand particles (Fig. 5D), creating a new soil porous matrix (Fig. 5C). Our results are consistent with previous studies where chitosan fibers were observed to form bridges among soil particles (Hataf et al., 2018). Also, previous studies showed that root mucilage (e.g. hydrogel-like material from plant roots exudates) between soil particles changed soil structure (Benard et al., 2017; Benard et al., 2018). In this case, where there was low mucilage concentration, the bridges presented 1D isolated filaments (i.e. hollow cylinders) and, when mucilage concentration increased, the filaments created 2D structures that modified the hydraulic behavior of the soil-root interface, maintaining

the continuity of the liquid phase across the rhizosphere (Benard et al., 2017; Benard et al., 2018). Our results from microscopy images from the bacterial alginate treatment (Fig. 5C) are similar to those found previously about the formation of dried chitosan fibers and drying mucilage (Benard et al., 2018; Hataf et al., 2018). Drying conditions generate the evaporation of water contained in the links of the hydrogel-sand interface, shrinking the liquid bridges and increasing the surface to volume ratio and finally modifying the hydrogel-sand particles interactions (Benard et al., 2018). Nevertheless, we found clear differences in the Ca-alginate hydrogel treatment compared with our bacterial alginate treatment and previously reported dried chitosan, fibers, and dried mucilage (Fig. 5C and Fig. 6B; Hataf et al., 2018; Benard et al., 2018). The results presented here showed not only 1D or 2D dehydrated bridges linking the particles (Benard et al., 2018; Hataf et al., 2018), but a new 3D matrix that creates new pores at inter-particle level, capable of creating micro and macro aggregates (Fig. 6C). This new finding could be comparable with the exudates of plant roots that modifies the soil mechanical and hydraulic behavior of the rhizosphere (Ahmed et al., 2014; Carminati et al., 2016; Benard et al., 2017; Galloway et al., 2018; Benard et al., 2018; Ahmed et al., 2018).

Hydraulics data revealed that treatments Ca-alginate hydrogel and bacterial alginate reduced almost in half the hydraulic conductivity compared to the control; improving the water retention capacity of the coarse quartz sand (Hataf et al., 2018; Wen et al., 2019). High hydraulic conductivity was shown in the control and calcium hydroxide treatments (Fig. 4), mainly because of the grain size diameter of coarse quartz sand (Fig. 1), defined as a coarse grained and poorly graded (SP) according to Unified Soil Classification System (USCS,1986). Quartz sand is not aggregated since the ratio of macro and microaggregates is unbalanced (i.e. more macro aggregates than micro aggregates) and it is well known that aggregates affect significantly the hydraulic behavior of soils (Huang, Li, and Summer, 2012; Carminati et al., 2012; Galloway et al., 2018; Benard et al., 2019). In here, this coarse quartz sand displayed a non-linear Forchheimer flow regime with relatively high Reynolds and Forchheimer numbers (i.e. Re ≈12.0, F0 ≈2.5) and a non-Darcy effect of E ≈ 0.7 (Bear, 1972; Comiti et al., 2000; Zeng and Grigg, 2006; Huang and Ayoub, 2008). The Ca-alginate hydrogel and bacterial alginate was found to have an effect on the

mechanics of the fluid phase of treated coarse quartz sand by shifting the flow regime from non-linear where inertial forces dominate to linear where viscous forces dominate. This relates well with our estimation of the Oh number that indicates that the sand treated with Ca-alginate hydrogel and bacterial alginate increase the viscous forces, helping to maintain the hydraulic connectivity across the soil. This is particularly important during soil drying, since having a large Oh number (Oh >> 1) allows the hydrogel filaments in the soil to be kept more rigid due to the considerable increase in their viscosity, maintaining the water stored within the filamentous network; water that can be beneficial in agricultural contexts facing low available water capacity (Bernard et al., 2018; Benard et al., 2019). Previous studies have documented changes in the arrangement of soil particles and aggregates due to plants and microorganism activity that release exopolysaccharides (EPS) to the surrounding soil; providing a gluing effect and modifying the soil matrix (Zhao, 2014; Benard et al., 2018; Galloway et al., 2018; Benard et al., 2019). The results presented here are consistent with previous research where different hydrogel concentration were used, showing a significant reduction in the hydraulic conductivity of sand with different sodium alginate content (i.e. seaweed alginate; Wen et al., 2019). Our research shows that Ca-alginate hydrogel and bacterial alginate treatments reduce the water movement between 2.7-3.7 times. On the other hand, the data suggest that the hydraulic behavior of the coarse quartz sand can be modified by the incorporation of bacterial alginate and Ca-alginate hydrogel treatments, which could simulate the effect of natural polysaccharides excreted by microorganisms, and mucilage from root plants (Ahmed et al., 2014; Ahmed et al., 2015; Galloway et al., 2018; Benard et al., 2018; Benard et al., 2019).

The stability of soil aggregates plays a key role on the soil storage and movement of water (i.e. hydraulic conductivity), soil aeration, soil erosion, soil microbiological activity, and root growth of plants (Kramer and Boyer, 1995; Amézketa, 1999; Carminati et al., 2008; Carminati and Flühler, 2009; Carminati et al., 2012; Heinse et al., 2015; Le Bissonnais, 2016; Galloway et al., 2018). In this study we used coarse quartz sand to quantify the real effect of the Ca-alginate hydrogel on the aggregate stability of soil. The quartz sand used in this investigation showed no soil aggregates, and the grain size diameter were composed mainly in

the range from 500 μm to 125 μm (see Fig. 1). Nevertheless, our results showed a significant improvement in the MWD (mm/g) measurement with the Ca-alginate hydrogel treatment (1.5) compared with the control, calcium, and even bacterial alginate treatments. According to the classes of stability and crustability presented by Le Bissonnais (2016), the control, calcium, and bacterial alginate treatments used here display very *unstable* stability (< 0.4 MWD). Soils in this class (i.e. very unstable stability of soil aggregates) are more susceptible to physical-disruptive environmental phenomena such as erosion and runoff and have higher water permeability (i.e. high hydraulic conductivity and low water holding capacity; De Ploey and Poesen, 1985; Amézketa, 1999; Carminati et al., 2008). On the other hand, the Ca-alginate hydrogel treatment presented a MWD (mm/g) value classified as *stable* stability (1.3-2.0); providing strong evidence that Ca-alginate hydrogel helped to create aggregates in coarse-size sand. We think that these results are explained by the new 3-D matrix created between the coarse quartz sand particles (Fig. 5D, 6C). The 3-D matrix modifies the physical contact between the coarse quartz sand particles, altering the macro and micro-pores, air pockets, and water held between them (Fig. 6C). It is important to note that the bacterial alginate treatment did have an important effect in enhancing the mechanical and hydraulic behavior of coarse quartz sand. Our schematic illustration summarizes the presence of bacterial alginate filaments and bacterial alginate hollow cylinders (Fig. 6B) that might be enough to have an impact and change the situation observed in the control and coarse quartz treatment (Fig. 6A). However, further experiments should focus on more complex and reactive soil matrices, expanding the results from this work. Finally, in further studies at field level, different concentrations of bacterial alginate with different molecular composition (e.g. molecular weight, acetylation degree, and G/M ratios) should be considered.

6. CONCLUSSION

We studied the effects of a new hydrogel based on bacterial alginate on the mechanics and hydraulics of coarse-sized sand. Mechanical (i.e. soil strength, aggregate stability) and hydraulic behavior (hydraulic conductivity) were modified and improved by creating a new hydrogel sand porous material. Our results suggest that bacterial alginate-based hydrogel applied to sandy soils might be useful in

mitigating the negative impacts of climate change in agricultural contexts (i.e. wind erosion, flooding, drought). However, future experiments should investigate changes in the mechanical behavior of soils with different textural classes, and organic components (i.e. organic matter), including the dynamics of hydraulic behavior under different load stresses. Furthermore, the interaction of the bacterial alginate-based hydrogel with biological material systems (i.e. root plants) and the hydraulics involved in the soil-hydrogel-root interface are still poorly understood and should be further investigated. To assess the suitability of these composites as a soil improver, further work should include biophysical studies in this complex coarse quartz sand. Filling these gaps of knowledge about the effects of the bacterial alginate-based hydrogel on the soil-plant-atmosphere continuum (SPAC) might help to better understand how to manage agricultural systems subjected to the negative effects of climate change, allowing to mitigate major droughts and help in soil conservation efforts.

7. ACKNOWLEDGEMENTS

This study was carried out with funding from the Chilean National Agency for Research and Development (ANID), within the Fondecyt grant Nº11180102. Authors gratefully acknowledges the “Research Nucleus on Climate Change and Protected Agriculture", VRIEA-PUCV grant 039.426/2020. We kindly thank Excequel Ponce for his technical assistance. Finally, we thank the company MIGRIN S.A. for the sand material.

8. AUTHOR CONTRIBUTIONS

Cesar Barrientos-Sanhueza: Conceptualization; Data curation; Formal Analysis; Investigation; Methodology; Writing-original draft; Writing-review & editing. Pedro Mondaca: Investigation; Methodology. Miguel Tamayo: Investigation; Methodology. Juan E. Álvaro: Resources; Writing-review & editing. Alvaro Díaz-Barrera: Conceptualization; Resources; Writing-review & editing. Italo F. Cuneo: Conceptualization; Formal Analysis; Project Administration; Supervision; Writing-original draft; Writing-review & editing

8. CONFLICTS OF INTERESTS

The authors declare that this research was conducted in the absence of any commercial or financial relationships that could be constructed as a potential conflict of interest.

REFERENCES

Ahmed, M., Kroener, E., Benard, P., Zarebanadkouki, M., Kaestner, A., Carminati, A. 2015. Drying mucilage causes water repellency in the rhizosphere of maize measurements and modeling. Plant Soil 407, 161–171.

Ahmed, M., Kroener, E., Holz, M., Zarebanadkouki, M., Carminati A. 2014. Mucilage exudation facilitates root water uptake in dry soils. Funct. Plant Biol. 41 (11), 1129-1137.

Ahmed, M.A., Zarebanadkouki, M., Ahmadi, K., Kroener, E., Kostka, S., Kaestner, A., Carminati, A. 2018. Engineering rhizosphere hydraulics: Pathways to improve plant adaptation to drought. Vadose Zone J. 17, 1-12.

Alameda, D., Anten, N. P. R., Villar, R. 2012. Soil compaction effects on growth and root traits of tobacco depend on light, water regime and mechanical stress. Soil Till. Res. 120, 121–129.

Aleklett, K., Kiers, E., Ohlsson, P., Shimizu, T. S., Caldas, V. EA., Hammer, E. C. 2018. Build your own soil: exploring microfluidics to create microbial habitat structures. ISME J. 12, 312–319.

Amézketa, E. 1999. Soil Aggregate Stability: A Review. J. Sustain Agr. 14(2-3), 83–151.

ASTM C136/C136M-14. Standard Test Method for Sieve Analysis of Fine and Coarse Aggregates, ASTM International, West Conshohocken, PA, 2014.

ASTM-D5084-16a. Standard Test Method for Measurement of Hydraulic Conductivity of Saturated Porous Materials using a Flexible Wall Permeameter, ASTM International, West Conshohoken, PA, 2016.

Barnes, R.T., Gallagher, M.E., Masiello, C.A., Liu, Z., Dugan, B. 2014. Biochar-Induced Changes in Soil Hydraulic Conductivity and Dissolved Nutrient Fluxes Constrained by Laboratory Experiments. PLoS ONE 9(9): e108340.

Barzegar, A., Asoodar, M., Khadish, A., Hashemi, A., Herbert, S. 2003. Soil physical characteristics and chickpea yield responses to tillage treatments. Soil Till. Res. 71(1), 49–57.

Bear, J. 1972. Dynamics of Fluids in Porous Media. Elsevier, New York (1972)

Benard, P., Zarebanadkouki, M., Brax, M., Kaltenbach, R., Jerjen, I., Marone, F., Couradeau, E., Felde, V.J.M.N.L., Kaestner, A., Carminati, A. 2019. Microhydrological niches in soils: How mucilage and EPS alter the biophysical properties of the rhizosphere and other biological hotspots. Vadose Zone J. 18. Doi: https://doi.org/10.2136/vzj2018.12.0211

Benard, P., Zarebanadkouki, M., Carminati, A. 2018. Game changer in soil science physics and hydraulics of the rhizosphere network. J. Plant Nutr. Soil Sci. 000, 1–4.

Benard, P., Zarebanadkouki, M., Hedwig, C., Holz, M., Ahmed, M.A., Carminati, A. 2017. Pore-scale distribution of mucilage affecting water repellency in the rhizosphere. Vadose Zone J. 17, 1-9.

Borrelli, P., Robinson, D., Fleischer, L., Lugato, E., Ballabio, C., Alewell, C., Meusburger, K., Modugno, S., Schütt, B., Ferro, V., Bagarello, V., Van Oost, K., Montanarella, L., Panagos, P. 2017. An assessment of the global impact of 21st century land use change on soil erosion. Nat. Commun. 8, Article number: 2013.

Bronick, C.J., Lal, R. 2005. Soil structure and management: a review. Geoderma 124, 3-22.

Cao, Y., Wang, B., Guo, H., Xiao, H., Wei, T. 2017. The effect of super absorbent polymers on soil and water conservation on the terraces of the loess plateau. Ecol. Eng. 102, 270-279.

Carminati, A., Flühler, H. 2009. Water infiltration and redistribution in soil aggregate packings. Vadose Zone J. 8,150–157.

Carminati, A., Kaestner, A., Lehmann, P., Flühler, H. 2008. Unsaturated water flow across soil aggregate contacts. Adv. Water Resour. 31, 1221–1232.

Carminati, A. 2012. A model of root water uptake coupled with rhizosphere dynamics. Vadose Zone J. 11. Doi: 10.2136/vzj2011.0106.

Carminati, A., Zarebanadkouki, M., Kroener, M., Ahmed, A., Holz, M. 2016. Biophysical rhizosphere processes affecting root water uptake. Ann. Bot. 118 (4), 561–571.

Chang, I., Cho, G.C. 2012. Strengthening of Korean residual soil with b-1,3/1,6-glucan biopolymer. Constr. Build Mater. 30, 30–35.

Chang, I., Im, J., Cho, G-C. 2016. Geotechnical engineering behaviors of gellan gum biopolymer treated sand. Can. Geotech. J. 53(10), 1658-1670.

Chang, I., Im, J., Prasidhi, A., Cho, G.C. 2015. Effects of Xanthan gum biopolymer on soil strengthening. Constr. Build Mater. 74, 65–72.

Chang, I., Prasidhi, A.K., Im, J., Shin, H., Cho, G. 2015. Soil treatment using microbial biopolymers for anti-desertification purposes. Geoderma 253–254, 39–47.

Comiti, C., Sabiri, N.E., Montillet, A. 2000. Experimental characterization of flow regimes in various porous media - III: limit of Darcy's or creeping flow regime for Newtonian and purely viscous non-Newtonianfluids. Chem. Eng. Sci. 55, 3057–3061.

Dasari, S., Ganjayi, M.S., Meriga, B. 2018. Glutathione S-transferase is a good biomarker in acrylamide induced neurotoxicity and genotoxicity. Interdiscip. Toxicol. 11(2), 115-121.

De Ploey, J., Poesen, J. 1985. Aggregate stability, runoff generation and interrill erosion. In: Geomorphology and Soils (eds K.S. Richards, R.R. Arnett & S. Ellis), pp. 99–120. Allen and Unwin, London.

Díaz-Barrera, A., Soto, E. 2010. Biotechnological uses of Azotobacter vinelandii: Current state, limits and prospects. Afr. J. Biotechnol. 9, 5240-5250.

Díaz‐Barrera, A., Maturana, N., Pacheco‐Leyva, I., Martínez, I., Altamirano, C. 2017. Different responses in the expression of alginases, alginate polymerase and acetylation genes during alginate production by Azotobacter vinelandii under oxygen‐controlled conditions. J. Ind. Microbiol. Biot. 44, 1041–1051.

Draget, K.I., Smidsrød, O., Skjåk-Bræk, G. 2005. Alginates from algae. In: Steinbüchel A, Rhee SK, editors. Polysaccharides and polyamides in the food industry: properties, production, and patents. 1-30.

Food and Agriculture Organization (FAO). 2003. Codex Alimentarius commission: Joint FAO/WHO Food standards program Codex Committee and Food additives and Food contaminants. Rotterdam. The Netherlands.

Fox, J., Weisberg, S. 2011. An R companion to applied regression, 2nd edn. Thousand Oaks CA: Sage. [WWW document] URL http://socserv.socsci.mcmaster.ca/jfox/Books/Companion [accesed 20 january 2020].

Galloway, A.F., Pedersen, M.J., Merry, B., Marcus, S.E., Blacker, J., Benning, L.G., Field, K., Knox, J.P. 2018. Xyloglucan is released by plants and promotes soil particle aggregation. New Phytol. 217(3), 1128–1136.

Garreaud, R., Alvarez-Garreton, C., Barichivich, J., Boisier, J., Christie, D., Galleguillos, M., LeQuesne, C., McPhee, J., Zambrano-Bigiarini, M. 2017. The 2010-2015 megadrought in central Chile: impacts on regional hydroclimate and vegetation. Hydrol. Earth Syst. Sci. 21, 6307–6327.

Ghezzehei, T. 2012. Soil Structure. In: Handbook of Soil Sciences: Properties and Processes (CRC Press, Taylor and Francis Group). 39-55.

Guilherme, M.R., Aouada, F.A., Fajardo, A.R., Martins, A.F., Paulino, A.T., Davi, M.F.T., Rubira, A.F., Muniz, E.C. 2015. Superabsorbent hydrogels based on polysaccharides for application in agriculture as soil conditioner and nutrient carrier: A review. Eur. Polym. J. 72, 365-385.

Hataf, N., Ghadir, P., Ranjbar, N. 2018. Investigation of soil stabilization using chitosan biopolymer. J. Clean. Prod. 170, 1493-1500.

Heinse, R., Jones, S.B., Or, D., Podolskiy, I., Topham, T.S., Poritz, D., Bingham, G.E. 2015. Microgravity Oxygen Difussion and Water Retention Measurements in Unsaturated Porous Media aboard the International Space Station. Vadose Zone J. 14(6), 1-19.

Hillel, D., 2003. Introduction to Environmental Soil Physics. Academic press, California.

Horn, R., Peth, S. 2012. Mechanics of Unsaturated Soils for Agricultural Applications. In: Handbook of Soil Science: Properties and Processes (CRC Press, Taylor and Francis Group). 57-86.

Huang, H., Ayoub, J. 2008. Applicability of the Forchheimer equation for non-Darcy flow in porous media. SPEJ. 13, 112–122.

Huang, P., Li, Y., Summer, M. 2012. Hanbook of Soil Sciences: Properties and Processes (CRC Press, Taylor and Francis Group).

Keersebilck, N.C. 1990. Erosion control in the tropics. In: Soil colloids and their Associations in Aggregates (SpringerScience+Business Media New York). 567-575.

Keller, T., Défosse, P., Weisskopf, P., Arvidsson, J., Richard, G. 2007. SoilFlex: A model for prediction of soil stresses and soil compaction due to agricultural field traffic including a synthesis of analytical approaches. Soil Tillage Res. 93(2), 391–411.

Konings, E.J., Baars, A.J., van Klaveren, J.D. 2003. Acrylamide exposure from foods of the Dutch population and an assessment of the consequent risks. Food Chem Toxicol. 41(11), 1569-1579.

Kramer, P.J., Boyer, J.S. 1995. Water relations of plant and soil (Academic Press, San Diego).

Krainer, S., Smit, C., Hirn, U.2019. The effect of viscosity and surface tension on inkjet printed picoliter dots. RSC Adv. 9, 31708–31719

Kumar, A., Saha, A. 2011. Effect of polyacrylamide and gypsum on surface runoff, sediment yield and nutrient losses from steep slopes. Agric. Water Manag. 98(6), 999–1004.

Lai, S.M., Gu, Z.T., Zhao, M.M. 2017. Toxic effect of acrylamide on the development of hippocampal neurons of weaning rats. Neural Regen Res. 12(10), 1648-1654.

Lal, R. 2001. Assesment Methods for Soil Carbon. Advances in Soil Science. CRC Press, 403-416. Boca Raton, Fl.

Le Bissonnais, Y. 2016. Aggregate stability and assessment of soil crustability and erodibility: I. Theory and methodology. Eur. J. Soil Sci. 67, 11-21.

Leal, D., Matsuhiro, B., Rossib, M., Carusoc, F. 2008. FT-IR spectra of alginic acid block fractions in three species of brown seaweeds. Carbohydr. Res. 343, 308–316.

Leite, M.H., Ferland, F. 2001. Determination of unconfined compressive strength and Young's modulus of porous materials by indentation tests. Eng. Geol. 59(3–4):267–80

Lentz, R. D. 2015. Polyacrylamide and biopolymer effects on flocculation, aggregate stability, and water seepage in a silt loam. Geoderma 241-242, 289–294.

Liu, X., Chan, Z. 2015. Application of potassium polyacrylate increases soil water status and improves growth of bermudagrass (Cynodon dactylon) under drought stress condition. Sci. Hortic. 197, 705-711.

Lu, S., Wang, Z., Hu, Y., Liu, B., Liu, J.E. 2018. Effectiveness and durability of polyacrylamide (PAM) and polysaccharide (Jag C 162) in reducing soil erosion under simulated rainfalls. Water 10, 257.

Lyles, L. 1977. Wind Erosion: Processes and Effect on Soil Productivity. Transactions of the ASAE 20(5), 0880–0884.

Menon, M., Mawodza, T., Rabbani, A., Blaud, A., Lair, G.J., Babaei, M., Kercheva, M., Rousseva, S., Banwart, S., 2020. Pore system characteristics of soil aggregates and their relevance to aggregate stability. Geoderma 366, 114259.

Narjary, B., Aggarwal, P. 2014. Evaluation of Soil Physical Quality under Amendments and Hydrogel Applications in a Soybean–Wheat Cropping System, Commun. Soil Sci. Plan. 45(9), 1167-1180.

Narjary, B., Aggarwal, P., Singh, A., Chakraborty, D., Singh, R. 2012. Water availability in different soils in relation to hydrogel application. Geoderma 187-188, 94-101.

Obrzud, R., Truty, A. 2012. The Hardening soil model: A practical model – A practical guidebook Z soil. PC 100701 report, revised 21.10.2018.

Padilla-Córdova, C., Mongili, B., Contreras, P., Fino, D., Tommasi, T., Díaz-Barrera, A. 2020. Productivity and scale-up of poly(3-hydroxybutyrate) production under different oxygen transfer conditions in cultures of Azotobacter vinelandii. J. Chem. Technol. Biot. Doi: 10.1002/jctb.6465.

Pawar, S. N., Edgar, K. J. 2012. Alginate derivatization: A review of chemistry, properties and applications. Biomaterials 33(11), 3279–3305.

Philip, J.R. 1966. Plan water relations: Some physical aspects. Ann. Rev. Plant Physiol. 17, 245–268.

Pimentel, D., Burgess, M. 2013. Soil Erosion Threatens Food Production. Agriculture 3, 443-463.

Rabot, E., Wiesmeier, M., Schlüter, S., & Vogel, H.-J. 2018. Soil structure as an indicator of soil functions: A review. Geoderma, 314, 122–137.

Radcliffe, D.E., Šimunek, J. 2012. Water flows in soils. In: Handbook of Soil Sciences: Propierties and Processes (CRC Press, Taylor and Francis Group). 115-148.

Sartori, C., Finch, DS., Ralph, B. 1997. Determination of the cation content of alginate thin films by FTIR spectroscopy. Polymer. 38(1):43-51.

Sikorski, P., Mo, F., Skjåk-Bræk, G., Stokke, B.T. 2007. Evidence for egg-box-compatible interactions in calcium-alginate gels from fiber X-ray diffraction. Bio-macromolecules 8, 2098-2103.

Singh, V.P., Yadav, S., Yadava, R.N. 2018. Climate change impacts. Water Science and Technology library. Springer Nature 82.

Stephen, H., Stephen, T. 1962. Binary Systems: Solubilities of Inorganic and Organic Compounds, Volume 1 P1. Elsevier Science.

Stewart, D., Rupp, D.E., Abou Najm, M.R., Selker J.S. 2016. A unified model for soil shrinkage, subsidence, and cracking. Vadose Zone J. 15. Doi:10.2136/vzj2015.11.0146.

Schlüter, S., Smmartino, S., Koestel, J. 2020. Exploring the relationship between soil structure and soil functions via pore-scale imaging. Geoderma 370, 114370.

Tatarko, J. 2001. Soil Aggregation and Wind Erosion: Processes and Measurements. Ann. Arid Zone 40, 251-263.

Taylor, H.M., Ratliff, L.F. 1969. Root elongation rates of cotton and peanuts as a function of soil strength and soil water content. Soil Sci. 108, 113-119.

Urtuvia, V., Maturana, N., Acevedo, F., Pena, C., Díaz-Barrera, A. 2017. Bacterial alginate production: an overview of its biosynthesis and potential industrial production. World J. Microb. Biot. 33, 198.

Verruijt, A. 2018. An introduction to Soil Mechanics: Theory and Applications of Transport in Porous Media. Springer Nature.

Vicuña, S., McPhee, J., Garreaud, R.D. 2012. Agriculture vulnerability to climate change in a snowmelt-driven basin in semiarid Chile. J. Water Res. Plan-Asce 138, 431-441.

Wen, K., Li, Y., Huang, W., Armwood, C., Amini, F., Li, L. 2019. Mechanical behaviors of hydrogel-impregnated sand. Constr. Build Mater. 207, 174-180.

Weston, D.P., Lentz, R.D., Cahn, M.D., Ogle, R.S., Rothert, A.K., Lydy, M.J. 2009. Toxicity of anionic polyacrylamide formulations when used for erosion control in agriculture. J. Environ. Qual. 38, 238-247.

Xu, S., Zhang, L., McLaughlin, N.B., Mi, J., Chen, Q., Liu, J. 2015. Effect of synthetic and natural water absorbing soil amendment soil physical properties under potato production in a semi-arid region. Soil Till. Res. 148, 31-39.

Zeng, Z., Grigg, R. 2006. A criterion for non-Darcy flow in porous media. Transp. Porous Media 63, 57–69.

Zhao, X. 2014. Multi-scale multi-mechanism design of tough hydrogels: building dissipation into stretchy networks. Soft Matter 10(5), 672–687.

FIGURE LEGENDS

FIGURE 1. Particle distribution curve of coarse quartz sand (MIGRIN S.A. non-metallic mining) used in the study. The coefficient of uniformity and gradation are 2.36 and 0.88, respectively. The sand belongs to a coarse grained and poorly graded (SP) type.

Figure 1

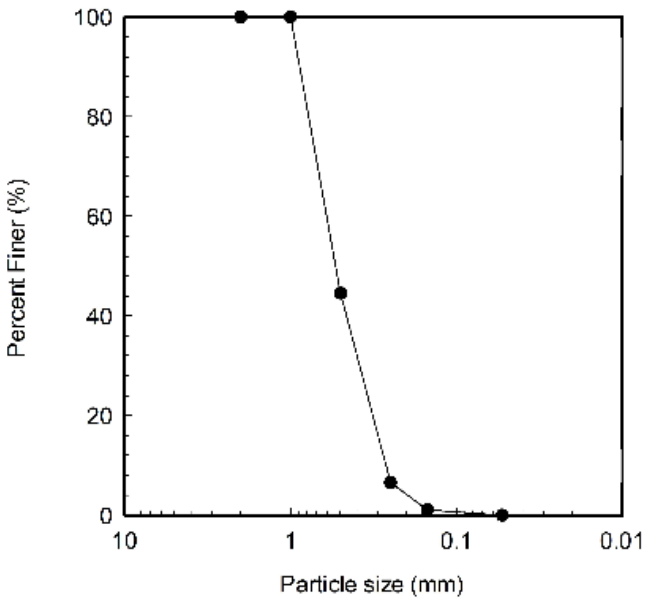

FIGURE 2. (A), Representative Stress-Strain diagram showing the unconfined uniaxial compression test of the coarse quartz sand treated with water (Control), calcium hydroxide ($Ca(OH)_2$) (Calcium) 0.5 M, bacterial alginate (Alginate) at 0.1% (w/w), and a mix of bacterial alginate and calcium hydroxide (Hydrogel). (B) The slopes show the representative Young´s elastic modulus in MPa of the coarse quartz sand under the four treatments. (C), Fracture of the sand cylinders (presented as % of axial strain at the final breakdown) were calculated with the slope angle (θ) of all experimental units. Data are mean ± SE (*n* = 6). Mean followed by different letters are significantly different at *P*<0.05.

Figure 2

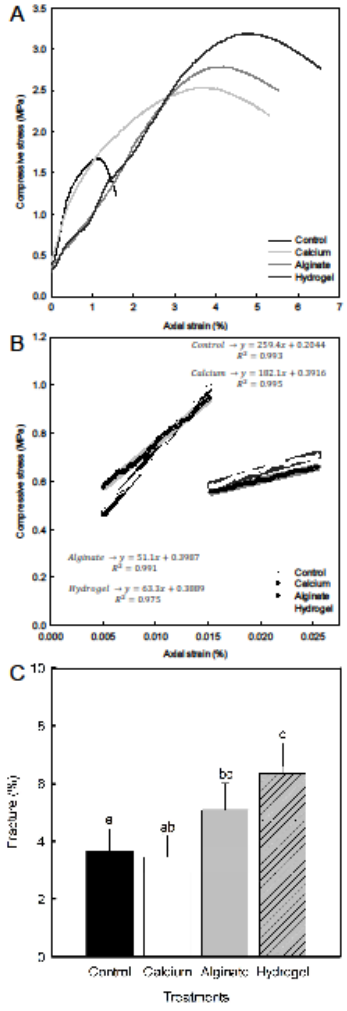

FIGURE 3. Effect of the different treatments on the aggregate stability of the coarse quartz sand. The response variable is shown as mean weight diameter (MWD). Data are means ± SE (*n* = 6). Mean followed by different letters are significantly different at P<0.05.

Figure 3

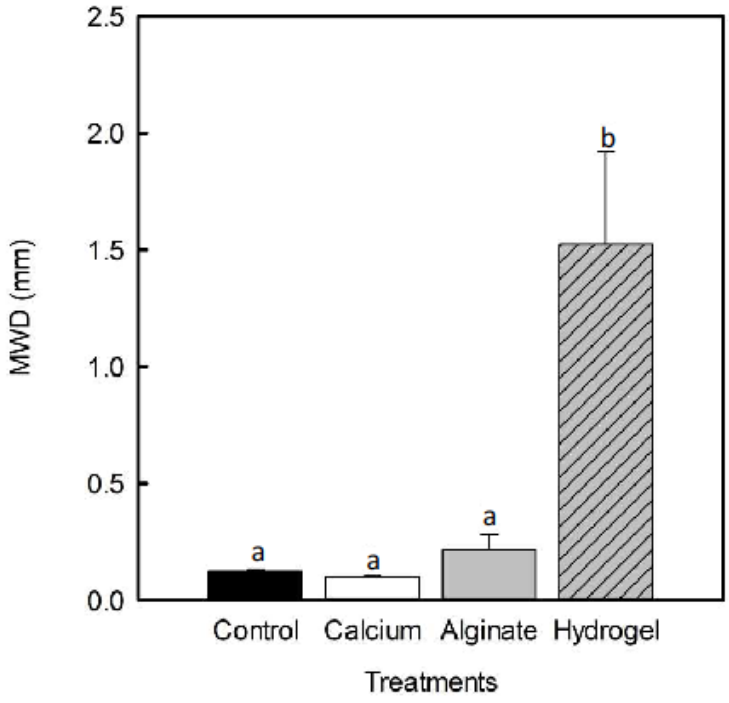

FIGURE 4. (A), Flux density-hydraulic gradient relationship showing that the bacterial alginate and hydrogel treatments lay on the linear part of the relation displaying low Reynolds numbers (Re~0.006) while the control and calcium treatments show a non-linear flow regime. (B), Hydraulic conductivity (k) of sand treated with water (Control), calcium hydroxide (Calcium) 0.5 M, bacterial alginate (Alginate) at 0.1% (w/w), and a mix of bacterial alginate and calcium hydroxide (Hydrogel) was obtained with the falling head permeability test. Data are means ± SE (n = 6). Mean followed by different letters are significantly different at P<0.05.

Figure 4

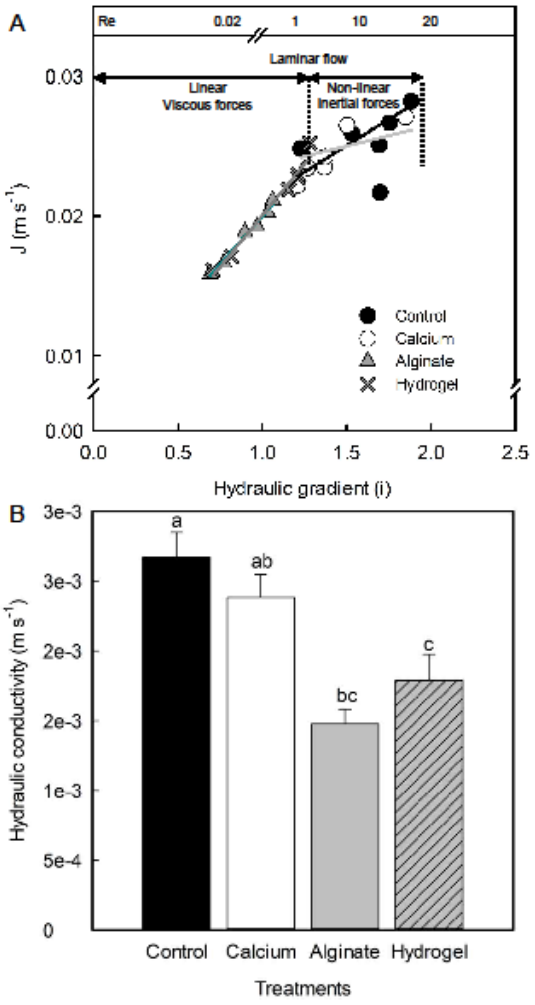

FIGURE 5. Transmission light microscopy images of treated sand with (A) control, (B) calcium, (C) bacterial alginate, and (D) hydrogel. Samples were covered with a mixture of the different treatments with a blue-ink solution to generate contrast. (a, b) arrows indicate the contact of the porous media particles and macropores formed between them. (c) arrows indicate the bacterial alginate links or "bridges" joining the sand particles. (d) arrows indicate the three-dimensional hydrogel matrix created among the sand particles. Bars = 500 µm. AP, air pocket; SP, sand particle; AL, bacterial alginate; HG, water-soluble hydrogel.

Figure 5

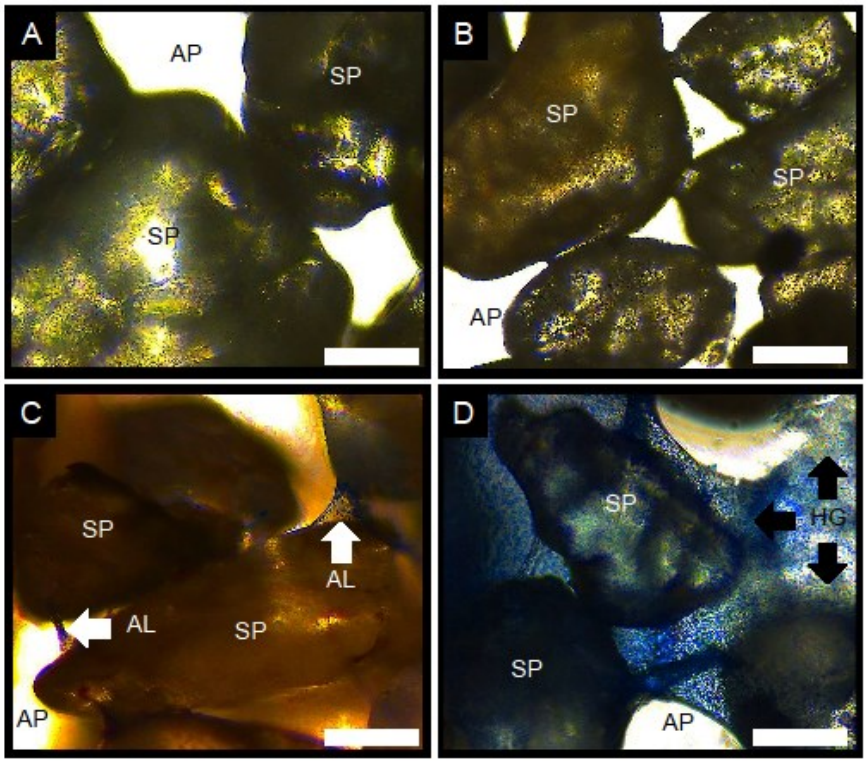

FIGURE 6. Schematic illustration model of coarse quartz sand particle interactions showing (a) the interaction of sand particles with DI water (Control), (b) interaction of sand particles with bacterial alginate modulated by the creation of alginate filaments and hollow cylinders, and (c) interaction of sand particles treated with hydrogel. In (c), the hydrogel creates a new porous matrix that can modify the macro and micro-pores and the mechanics of the fluid phase.

Figure 6